Journal of Alloys and Compounds 886 (2021) 161141

Contents lists available at ScienceDirect

Journal of Alloys and Compounds

journal homepage: www.elsevier.com/locate/jalcom

Boosting densification and microwave dielectric properties in cold sintered BaF_2 ceramics for 5.8 GHz WLAN applications

Ding Hao Jin[a], Bing Liu[a,c,*], Kai Xin Song[a,**], Kui Wen Xu[a], Yu Hui Huang[c], Cheng Chao Hu[b], Yuan Yun Hu[d]

[a] College of Electronic Information and Engineering, Hangzhou Dianzi University, Hangzhou, China
[b] College of Materials Science and Engineering, Liaocheng University, Liaocheng, China
[c] School of Materials Science and Engineering, Zhejiang University, Hangzhou, China
[d] Glead Electronics. Co., Ltd. Jiaxing, China

ARTICLE INFO

Article history:
Received 24 April 2021
Received in revised form 21 June 2021
Accepted 10 July 2021
Available online 14 July 2021

Keywords:
BaF_2
Cold sintering
Microwave dielectric ceramics
5.8 GHz WLAN

ABSTRACT

BaF_2 is a low-firing fluoride with excellent microwave dielectric properties, while the densification of BaF_2 ceramics is challenging via conventional sintering. In this work, dense BaF_2 ceramics with 95.3~98.5% relative densities have been prepared via the cold sintering (150–600 MPa, 150 °C, 1 h) and following post-annealing at 900 °C. The scanning electron microscope images demonstrate closely packed microstructures, and the chemical compatibility between BaF_2 ceramics and Ag electrodes is identified. The optimum *Qf* (82,320 GHz) is 1.53 times higher than that obtained via conventional sintering (53,654 GHz), with a dielectric permittivity, ε_r = 7.3, and a temperature coefficient of resonant frequency, τ_f = −107.9 ppm/°C. Furthermore, a BaF_2-based microstrip patch antenna is fabricated, which realizes an S_{11} = −16.5 dB, a high gain of 5.84 dB, and total efficiency of −0.38 dB at 5.78 GHz. The exceptional microwave dielectric properties and antenna performances indicate that BaF_2 ceramics are promising candidates for 5.8 GHz wireless local area network applications.

1. Introduction

The ongoing wave of network transformation is fueled by the rapid development of wireless communication technology. The rapidly deployable technology has given modern society the ability to extend networking communications in areas where traditional wiring may be too expensive or impossible. The wireless local area network (WLAN) is one of the most popular routes in constructing wireless networks. The carrier frequencies of WLAN include the lower-frequency band of 2.4 GHz (2.4–2.484 GHz) and the higher-frequency band of 5.8 GHz (5.725–5.825 GHz) [1,2]. Nowadays, the 2.4 GHz band is becoming crowded owing to the dramatic growth of wireless communication demands. Many users opt to use the 5.8 GHz band since it provides more spectrums and encounters less interference.

Microwave dielectric ceramics have established their status in wireless communication systems by improving the size and packaging density of microwave integrated circuits [3–5]. For antenna substrate applications, the crucial characteristics of microwave dielectric ceramics are low dielectric permittivity (ε_r), high quality factor (*Qf*), and near-zero temperature coefficient of the resonant frequency (τ_f). Besides, a low densification temperature (<960 °C) allows ceramics to cofire with conductive electrodes (such as Ag), offering the ability to be applied in the low temperature cofired ceramic (LTCC) technology [5–7].

According to the Clausius-Mossotti equation, ε_r is determined by the ionic polarizability per volume [8]. Hence, the search of the low-ε_r materials is mainly focused on oxides with low polarizabilities (such as silicates, aluminates, and borates [9–14]). Recently, researchers have expanded the low-ε_r materials to fluorides since F has a lower ionic polarizability of 1.62 $Å^3$ than that of O (2.01 $Å^3$) [15]. Geyer et al. prepared a series of fluoride single crystals and reported excellent dielectric performances at the microwave frequency range [16]. Zhang et al. reported a novel low-loss $Li_5Ti_2O_6F$ ceramics and identified their potential applications in LTCC technology [17]. Song et al. prepared the low-fired BaF_2 ceramics through conventional sintering (CS) at 925 °C and reported a low ε_r of 6.72 and an acceptable *Qf* value of 53,654 GHz [18]. Meanwhile, owing to the gas entrapment and the low driving force of densification during CS, the

* Corresponding author at: College of Electronic Information and Engineering, Hangzhou Dianzi University, Hangzhou, China.
** Corresponding author.
E-mail addresses: liubing@hdu.edu.cn (B. Liu), kxsong@hdu.edu.cn (K.X. Song).

https://doi.org/10.1016/j.jallcom.2021.161141
0925-8388/

optimal relative density of the conventional sintered BaF_2 ceramics was only 92.04%. [18]. Given that the porous microstructure is notoriously harmful to the *Qf* values, the optimization of densification in BaF_2 ceramics may trigger a breakthrough in the development of low-loss fluorides.

Cold sintering is a novel low-temperature consolidation technique that applies high pressures (hundreds of MPa) to accelerate the grain boundary/surface diffusion and mass transport [19,20]. Recent work on ultra-low temperature (below 200 °C) densification via cold sintering is mainly focused on components with high solubilities (usually in water), such as Li_2MoO_4 (44.8 g/100 mL), NaCl (36 g/100 mL), and H_3BO_3 (5.80 g/100 mL) [14,21,22]. For the insoluble compounds such as $BaTiO_3$, $K_{0.5}Na_{0.5}NbO_3$, and TiO_2, a following post-annealing treatment is generally required [23–25]. Hence, given the great potential of performance improvement and the low solubility (0.161 g/100 mL) of BaF_2 [26], BaF_2 ceramics are prepared via a cold sintering process followed by a subsequent post-annealing at 900 °C. The densification, microwave dielectric properties, and their chemical compatibility with Ag electrodes are systematically investigated. Moreover, a BaF_2-based microstrip antenna operating at 5.8 GHz is designed and fabricated to identify their potential WLAN applications. The return loss, radiation pattern, gain, and total efficiency of the BaF_2-based antenna are measured and compared with the simulated ones.

2. Experimental procedure

Prior to weighing, BaF_2 raw powder with high purity (99.99%) was placed into the oven and dried overnight at 150 °C. After drying, the powder was homogeneously mixed with 10 wt% of deionized water and then cold sintered under the pressures of 150–600 MPa. The unaxial pressure for the BaF_2 substrate was 600 MPa. The cold sintering temperature and dwelling time were fixed as 150 °C/1 h. The dimensions of the as-cold sintered pellets were 12.7 mm in diameter and ~5 mm in height. The as-cold sintered pellets were then post annealed at 900 °C for 3 h to achieve further densifications.

The relative density was evaluated using the Archimedes method. The room-temperature X-ray diffraction (XRD) patterns were recorded using a RIGAKU D/MAX 2550/PC diffractometer. The XRD data for Rietveld refinement was collected with a scanning step size of 0.02° and a counting time of 1 s. The microstructures of the polished and thermally etched (875 °C/1 h) surfaces of BaF_2 ceramics were observed using a Zeiss Sigma 300 scanning electron microscopy (SEM). The microwave dielectric properties and the S_{11} curve of the fabricated antenna were evaluated using a Keysight N5234B network analyzer. The measured resonant frequency of the BaF_2 ceramics was around 11 GHz. ε_r and τ_f values were measured using the parallel-plate method [11]. *Qf* value was evaluated using the resonant cavity method [12]. The design and simulation of the proposed antenna were conducted using the Computer Simulation Technology (CST) software. The radiation patterns were measured in a STIMO SG24 microwave anechoic chamber.

3. Results and discussion

The XRD patterns of BaF_2 raw powder and ceramics obtained under various uniaxial pressures are shown in Fig. 1(a). All the diffraction patterns can be well indexed based on the standard PDF card of BaF_2 (JCPDS #85–1342), indicating that no phase transformation occurs during the cold sintering and post-annealing processes. Moreover, the shape and position of each diffraction peak remain stable with the increasing uniaxial pressures, suggesting that the uniaxial pressure has little effect on the structural parameters. Rietveld refinement of the XRD data is conducted to further identify the crystal structure, and the results are shown in Fig. 2(b). The crystal structure of cubic BaF_2 with a space group of Fm-3m. is adopted as the structural model. The calculated pattern is in good agreement with the measured one, which can be confirmed from both the low amplitude of the different line and the satisfactory results of the reliability factors (R_p = 7.98%, R_{wp} = 11.3%, and χ^2 = 6.43).

The SEM images of BaF_2 ceramics obtained under various uniaxial pressures are shown in Fig. 2(a)–(d), respectively. Dense and uniform microstructures with distinct grain boundaries can be found in the present ceramics. Some tiny pores at the grain boundary junctions are observed in Fig. 2(a) and (b) and disappear under higher uniaxial pressures. The grain size distributions and average grain sizes are insensitive to the uniaxial pressure, which are identified from the distribution curves shown in Fig. 2(e-h). Furthermore, the cold-sintered BaF_2 ceramics and Ag colloids are cofired at 900 °C to identify the chemical compatibility between BaF_2 and metallic electrodes. Fig. 2(i) and (j) show the XRD pattern and SEM image of the BaF_2-Ag ceramics, respectively. The XRD pattern exhibits an independent existence of BaF_2 and Ag composites, and no other secondary phases are observed. Besides, the SEM image demonstrates a distinct boundary between the two phases, which is further confirmed by the concentration profiles on both sides of the interface. Hence, it is reasonable to conclude that BaF_2 ceramics exhibit excellent chemical compatibility with Ag electrodes, which is promising for applications in the LTCC technology.

Fig. 3 shows the variation of the relative density and microwave dielectric properties of BaF_2 ceramics. With increasing the uniaxial pressure, the relative density ascends progressively from 95.3% at 150 MPa to 98.5% at 600 MPa, indicating the crucial role of uniaxial pressure in improving the densification. ε_r increases from 7.05 at 150 MPa to 7.30 at 600 MPa, and all the values are higher than that obtained via CS (6.72). On the other hand, the variation of ε_r follows the same trend as the relative density, indicating that ε_r should be mainly dominated by the porosity (*P*). According to Penn et al., the porosity corrected permittivity (ε_{cor}) can be calculated using Eq. (1) to exclude the effects of porosity [27].

$$\varepsilon_r = \varepsilon_{cor}\left(1 - \frac{3P(\varepsilon_{cor} - 1)}{2\varepsilon_{cor} + 1}\right) \quad (1)$$

As shown in Table 1, the calculated ε_{cor} values remain stable at approximately 7.45, further demonstrating the decisive role of porosity in controlling ε_r.

The *Qf* value increases from 72,350 GHz at 150 MPa to 80,400 GHz at 300 MPa and remains relatively stable at higher pressures. The optimal *Qf* value (82,320 GHz) is 53.4% higher than that via CS (53,654 GHz) [18]. Since the present ceramics share the same chemical composition, the variation of the *Qf* value in this work should be dominated by the extrinsic parameters such as pores, grain boundaries, and secondary phases [28,29]. With the absence of impurities and apparent grain size change, the improvement of the *Qf* should be mainly ascribed to the enhancement of densification. The τ_f value varies relatively stable with the increasing uniaxial pressure, and all the values remain at approximately −106 ppm/°C. The optimal microwave dielectric properties (ε_r = 7.3, *Qf* = 82,320 GHz and τ_f = −109.4 ppm/°C) are obtained under the applied pressure of 600 MPa.

The major component of the WLAN system is the antenna. The microstrip patch antennas gain widespread popularity among antennas due to their merits of low cost, low profile, and easy fabrication [30,31]. Fig. 4(a) shows the schematic figure of the designed patch antenna. A rectangular BaF_2 ceramic with dimensions of 20 × 20 × 1 mm is adopted as the substrate. The patch, microstrip transmission line, and ground plane are made of commercial copper foil with a thickness of 0.06 mm. The dimensions of the patch (width (*w*) and length (*l*)) are calculated based on the following equations

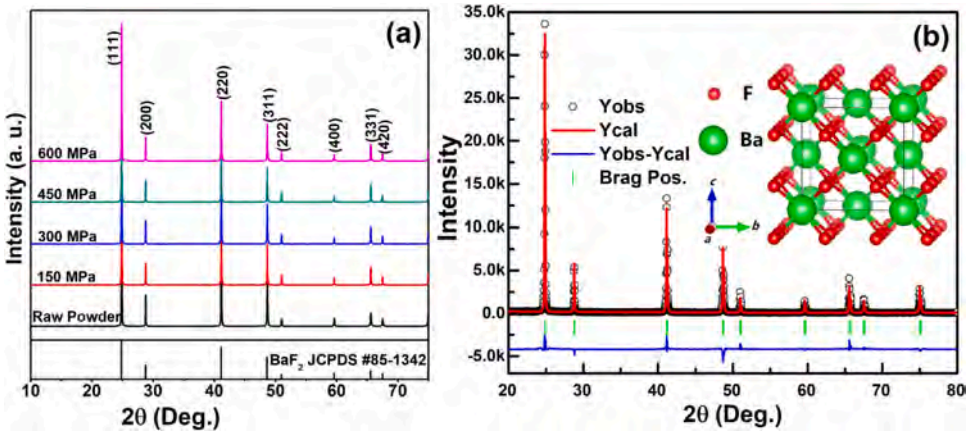

Fig. 1. (a) The XRD patterns of BaF_2 raw powder and ceramics in this work. (b) The measured (circles) and calculated (red lines) XRD patterns of BaF_2 ceramics obtained under the uniaxial pressure of 450 MPa. The inset shows the calculated crystal structure of BaF_2 ceramics.

and then trimmed based on the simulation results to achieve resonance at the desired 5.8 GHz [5].

$$w = \frac{c}{2f_0}\sqrt{\frac{2}{\varepsilon_r + 1}} \tag{2}$$

$$l = \frac{c_0}{2f_0\sqrt{\varepsilon_{eff}}} \tag{3}$$

$$\varepsilon_{eff} = \frac{\varepsilon_r + 1}{2} + \frac{\varepsilon_r - 1}{2}\left(\frac{1}{\sqrt{1 + 12H/w}}\right) \tag{4}$$

where, c is the velocity of light in vacuum, f_0 is the designed resonant frequency, ε_{eff} is the effective permittivity, and H is the substrate's height. The geometric dimensions and the front/rear views of the BaF_2-based antenna are shown in Fig. 4(a–c). The S parameters describe the input-output power relations and are the most commonly quoted parameters in evaluating the antenna performances. The measured and simulated S_{11} curves are plotted in Fig. 4(d). The S_{11} value defines the percentage of the power reflected from the antenna and is also known as the return loss. The measured S_{11} curve matches well with the simulated one, with the optimum value of −16.5 dB at the resonant frequency of 5.78 GHz. The measured resonant frequency is slightly lower than the simulated 5.80 GHz, which can be attributed to the fringing fields around the antenna [32]. S_{11} = −10 dB denotes that 90% of the power is radiated through the antenna. Hence, −10 dB is widely accepted as the base value for antenna applications. In this work, the BaF_2 based antenna presents a simulated −10 dB bandwidth of 152 MHz and a measured bandwidth of 96 MHz. According to Xiang et al., the difference in bandwidth can be ascribed to the ambient humidity and the SMA connector's soldering [5]. The Voltage Standing Wave Ratio (VSWR) is another crucial factor that numerically describes the impedance matching. The VSWR is always real and positive, and a value in the range of 1.0–1.5 is considered satisfactory for antenna applications. Fig. 4(e) plots the VSWR curve as a function of the frequency, where an excellent value of 1.35 is obtained at 5.78 GHz. Therefore, the fabricated antenna conforms to the expected properties and is compatible with the 5.8 GHz WLAN applications.

Fig. 5(a) shows the simulated upward and downward 3D far-field radiation patterns of the BaF_2-based antenna at 5.8 GHz. The fabricated antenna is a directional antenna with one main lobe radiating out from the patch side, and the maximum gain is 4.99 dB. The radiation patterns of the two principal planes (E- and H- planes) can be obtained by making two slices through the 3D pattern (*xoz* and *yoz* planes). Fig. 5(b, c) show the antenna measurement setup in the microwave anechoic chamber, where the radiation patterns are measured to compare with the simulated ones (see Fig. (d) and (e)). The measured and simulated patterns in both planes are in good agreement, where the maximum gain of 5.84 dB is measured at the

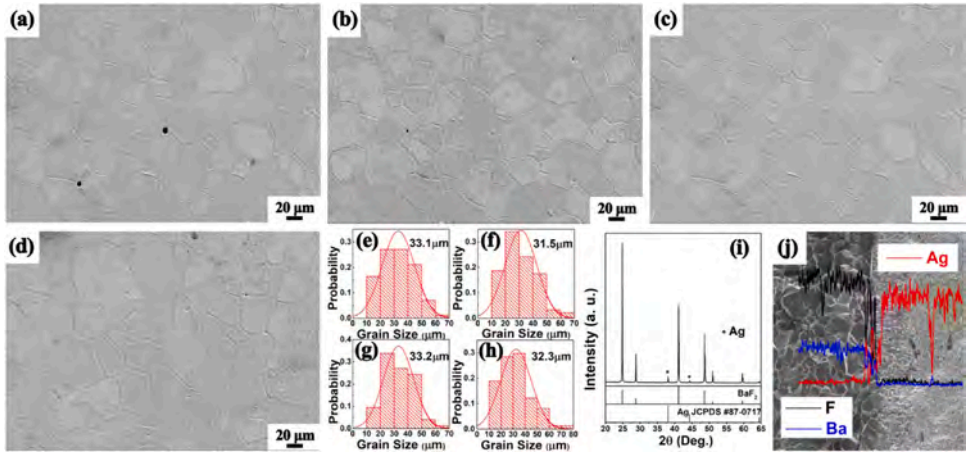

Fig. 2. Microstructures of BaF_2 ceramics prepared under various uniaxial pressures (a) 150 MPa, (b) 300 MPa, (c) 450 MPa, and (d) 600 MPa. (e-h) The corresponding grain size distributions and average grain sizes of Fig. (a)-(d). (i) XRD pattern and (j) SEM image and EDS (energy dispersive spectra) line scan result of BaF_2-Ag composite ceramics cofired at 900 °C.

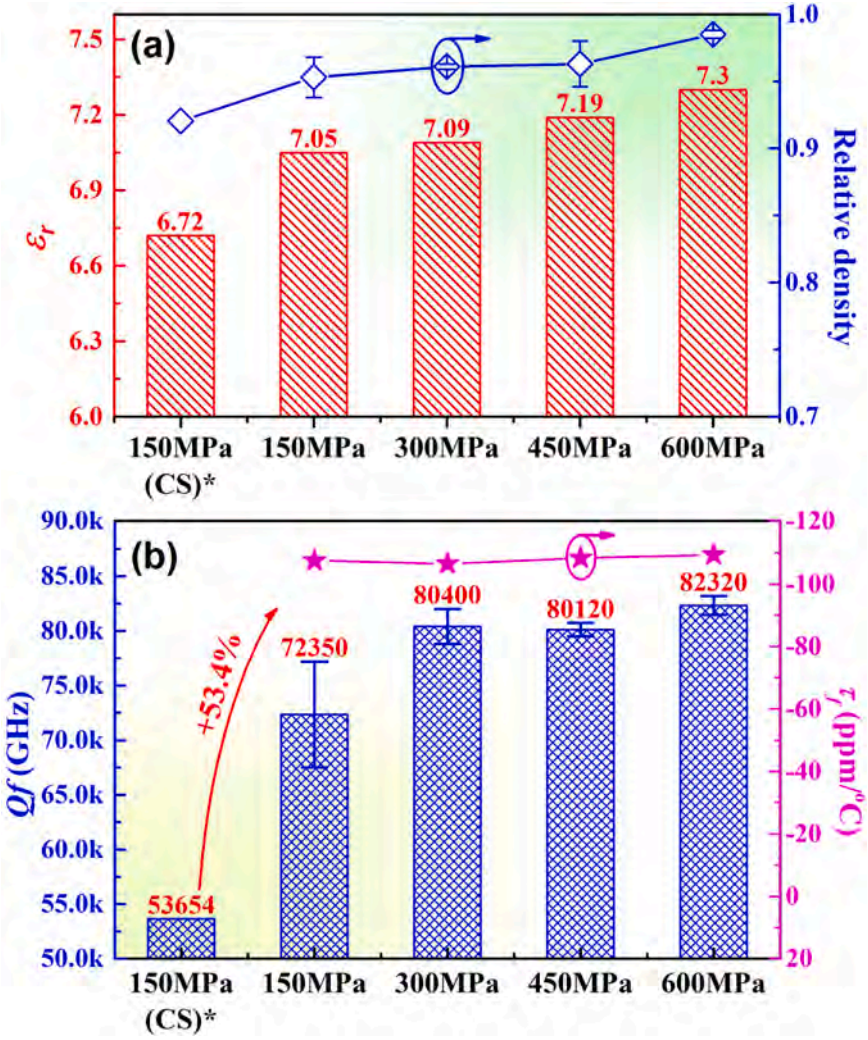

Fig. 3. (a) The relative density and ε_r of BaF_2 ceramics obtained under various uniaxial pressures. (b) The *Qf* and τ_f values of BaF_2 ceramics as functions of the applied uniaxial pressure. *The uniaxial pressure and microwave dielectric properties of the conventional sintered (CS) BaF_2 ceramics are cited from Ref. [18].

Table 1
The relative densities and microwave dielectric properties of BaF_2 ceramics in this work.

Uniaxial pressure	ρ	ε_r	ε_{cor}	*Qf* (GHz)	τ_f (ppm/°C)
CS-150 MPa	92.0%	6.72	7.44	53,654	−74.2
150 MPa	95.3%	7.05 ± 0.04	7.48	72,350 ± 4840	−107.5
300 MPa	96.1%	7.09 ± 0.03	7.44	80,400 ± 1600	−106.5
450 MPa	96.3%	7.19 ± 0.03	7.53	80,120 ± 610	−108.3
600 MPa	98.5%	7.3 ± 0.05	7.44	82,320 ± 870	−109.4

E-plane. The measured total efficiency of the BaF_2 antenna is plotted in Fig. 5(f), where the optimal value of −0.38 dB is obtained at 5.78 GHz. The total efficiency of an antenna is related to the power ratio using the following equation.

$$dB = 10 \times \lg(P_2/P_1) \quad (5)$$

where P_2 is the power being measured, and P_1 is the reference. According to Eq. (5), the fabricated BaF_2 antenna exhibits a power ratio

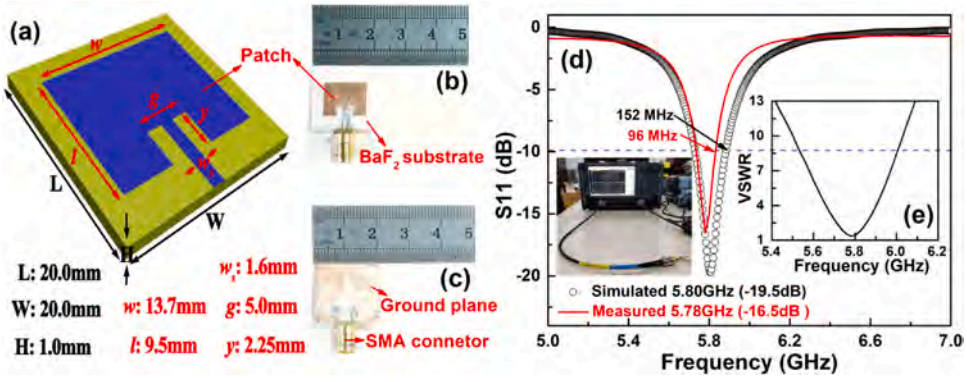

Fig. 4. (a) The dimensions and the (b) front and (c) rear views of the fabricated antenna. (d) The measured and simulated S_{11} curves of the fabricated antenna. The S_{11} curve is measured with the patch side upward (see the inset picture). (e) The VSWR curve in the frequency range of 5.4–6.2 GHz.

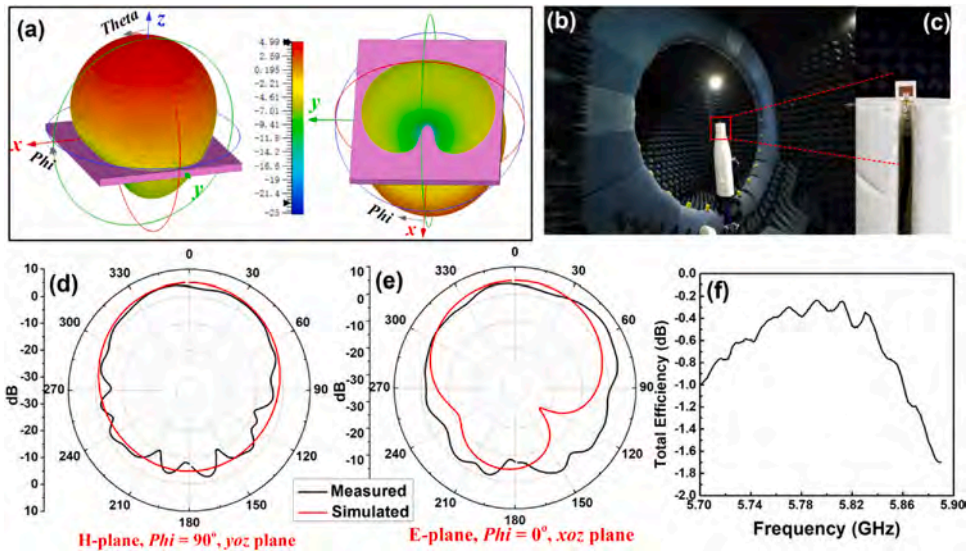

Fig. 5. (a) The simulated upward and downward 3D radiation patterns of the BaF_2-based antenna at 5.8 GHz. (b,c) The setup of antenna measuring devices in the microwave anechoic chamber. The measured and simulated radiation patterns at the (d) H-plane and (e) E-plane. (f) The measured total efficiency of the fabricated antenna as a function of the frequency.

of 91.6% at 5.78 GHz. The total efficiency of the commercial WiFi antennas is typically in the range of −7 to −1.5 dB (power ratio 20–70%). The excellent performance in the present work should be ascribed to the high *Qf* value of BaF_2 ceramics, as the total efficiency is sensitive to the dielectric loss of the substrates.

4. Conclusions

BaF_2 ceramics with 95.3~98.5% relative densities have been prepared via the cold sintering (150–600 MPa, 150 °C, 1 h) and following post-annealings at 900 °C. The XRD and EDS results demonstrate satisfactory chemical compatibility between BaF_2 ceramics and Ag electrodes, suggesting the great application prospects in the LTCC technology. The optimal microwave dielectric properties (ε_r =7.3, *Qf* = 82,320 GHz, and τ_f = −109.4 ppm/°C) are obtained under the applied uniaxial pressure of 600 MPa. The optimal *Qf* value is 1.53 times greater than for conventionally sintered BaF_2 ceramics (53,654 GHz). A BaF_2-based patch antenna is fabricated, which operates at 5.78 GHz with an S_{11} of −16.5 dB. Good agreements between the measured and simulated results are obtained, and the designed antenna exhibits a satisfactory gain and total efficiency of 5.84 dB and −0.38 dB, respectively. The excellent antenna performances conform to the expected properties, indicating that the cold sintered and post-annealed BaF_2 ceramics are promising candidates for 5.8 GHz WLAN applications.

CRediT authorship contribution statement

Ding Hao Jin: Investigation, Visualization. **Bing Liu:** Funding, Project administration, Supervision, Writing – review & editing. **Kai Xin Song:** Writing – review & editing. **Kui Wen Xu:** Software, Validation. **Yu Hui Huang:** Writing – review & editing. **Cheng Chao Hu:** Software, Validation. **Yuan Yun Hu:** Resources.

Declaration of Competing Interest

The authors declare that they have no known competing financial interests or personal relationships that could have appeared to influence the work reported in this paper.

Acknowledgments

This work was supported by the National Natural Science Foundation of China (Grant No. 51802062, 51802280), the Fundamental Research Funds for the Provincial Universities of Zhejiang under grant number of GK219909299001-408, the Postdoctoral Science Foundation of Zhejiang Province (Grant No. ZJ2020008), and the Program for Jiaxing Leading Innovative and Enterpreneurial Teams, China.

References

[1] T.V. Hoang, T.T. Le, Q.Y. Li, H.C. Park, Quad-band circularly polarized antenna for 2.4/5.3/5.8-GHz WLAN and 3.5-GHz WiMAX applications, IEEE Antenn. Wirel. Pr. 15 (2015) 1032–1035.
[2] R. Khanduri, S.S. Rattan, Performance comparison analysis between IEEE 802.11 a/b/g/n standards, Int. J. Comput. Appl. 78 (2013) 13–20.
[3] D. Wang, D. Zhou, S. Zhang, Y. Vardaxoglou, W.G. Whittow, D. Cadman, I.M. Reaney, Cold-sintered temperature stable $Na_{0.5}Bi_{0.5}MoO_4$–Li_2MoO_4 microwave composite ceramics, ACS Sustain. Chem. Eng. 6 (2018) 2438–2444.
[4] Y. Zhan, Yu Li L., Low-permittivity and high-Q value $Li_2Mg_3Ti_{1-x}(Zn_{1/3}Nb_{2/3})_xO_6$ microwave dielectric ceramics for microstrip antenna applications in 5G millimeter wave, J. Alloy. Compd. 857 (2021) 157608.
[5] H. Xiang, J. Kilpijärvi, S. Myllymäki, H. Yang, L. Fang, H. Jantunen, Spinel-olivine microwave dielectric ceramics with low sintering temperature and high quality factor for 5 GHz WiFi antennas, Appl. Mater. Today 21 (2020) 100826.
[6] M. Zhou, B. Tang, Z. Xiong, X. Zhang, S. Zhang, Effects of MgO doping on microwave dielectric properties of yttrium aluminum garnet ceramics, J. Alloy. Compd. 858 (2021) 158139.
[7] D. Zhou, L.X. Pang, D.W. Wang, Z.M. Qi, I.M. Reaney, High quality factor, ultralow sintering temperature $Li_6B_4O_9$ microwave dielectric ceramics with ultralow density for antenna substrates, ACS Sustain. Chem. Eng. 6 (2018) 11138–11143.
[8] P.V. Rysselberghe, Remarks concerning the Clausius-Mossotti law, J. Phys. Chem. 36 (2002) 1152–1155.
[9] L. Huang, S. Ding, X. Yan, T. Song, Y. Zhang, Structure and microwave dielectric properties of $BaAl_2Si_2O_8$ ceramic with Li_2O–B_2O_3 sintering additive, J. Alloy. Compd. 820 (2020) 153100.
[10] X.Q. Song, K. Du, Z. Zou, Z. Chen, W. Lu, S. Wang, W. Lei, Temperature-stable $BaAl_2Si_2O_8$–$Ba_5Si_8O_{21}$-based low-permittivity microwave dielectric ceramics for LTCC applications, Ceram. Int. 43 (2017) 14453–14456.
[11] B. Liu, C.C. Hu, Y.H. Huang, H.B. Bafrooei, K.X. Song, Crystal structure, infrared reflectivity spectra and microwave dielectric properties of $CaAl_2O_4$ ceramics with low permittivity, J. Alloy Compd. 791 (2019) 1033–1037.
[12] Y. Wu, C.C. Hu, B. Liu, Y.H. Huang, K.X. Song, Crystal structure, vibrational spectroscopy, and microwave dielectric properties of $CaAl_4O_7$ ceramics with low permittivity, J. Mater. Sci. Mater. Electron. 31 (2020) 4520–4526.
[13] L. Li, C.H. Liu, J.Y. Zhu, X.M. Chen, B_2O_3-modified fused silica microwave dielectric materials with ultra-low dielectric constant, J. Eur. Ceram. Soc. 35 (2015) 1799–1805.
[14] W.B. Hong, L. Li, H. Yan, S.Y. Wu, H.S. Yang, X.M. Chen, Room-temperature-densified H_3BO_3 microwave dielectric ceramics with ultra-low permittivity and ultra-high Qf value, J. Mater. 6 (2020) 233–239.

[15] R.D. Shannon, Dielectric polarizabilities of ions in oxides and fluorides, J. Appl. Phys. 73 (1993) 348–366.
[16] R.G. Geyer, J.B. Jarvis, J. Krupka, Dielectric characterization of single-crystal LiF, CaF_2, MgF_2, BaF_2, and SrF_2 at microwave frequencies, Proceedings of Annual Report Conference on IEEE Electrical Insulation and Dielectric Phenomena, 2004, CEIDP'04, 2004: 493–497.
[17] Z. Zhang, Y. Tang, H. Xiang, A. Yang, Y. Wang, C. Yin, Y. Tian, L. Fang, $Li_5Ti_2O_6F$: a new low-loss oxyfluoride microwave dielectric ceramic for LTCC applications, J. Mater. Sci. 55 (2020) 107–115.
[18] X. Song, K. Du, J. Li, X. Lan, W. Lu, X. Wang, W. Lei, Low-fired fluoride microwave dielectric ceramics with low dielectric loss, Ceram. Int. 45 (2019) 279–286.
[19] D. Wang, J. Chen, G. Wang, Z. Lu, S. Sun, J. Li, J. Jiang, D. Zhou, K. Song, I.M. Reaney, Cold sintered $LiMgPO_4$ based composites for low temperature cofired ceramic (LTCC) applications, J. Am. Ceram. Soc. 103 (2020) 6237–6244.
[20] H. Guo, A. Baker, J. Guo, C.A. Randall, Cold sintering process: a novel technique for low-temperature ceramic processing of ferroelectrics, J. Am. Ceram. Soc. 99 (2016) 3489–3507.
[21] W.B. Hong, L. Li, M. Cao, X.M. Chen, Plastic deformation and effects of water in room-temperature cold sintering of NaCl microwave dielectric ceramics, J. Am. Ceram. Soc. 101 (2018) 4038–4043.
[22] H. Kähäri, M. Teirikangas, J. Juuti, H. Jantunen, Dielectric properties of lithium molybdate ceramic fabricated at room temperature, J. Am. Ceram. Soc. 97 (2014) 3378–3379.
[23] H. Guo, J. Guo, A. Baker, C.A. Randall, Hydrothermal-assisted cold sintering process: a new guidance for low-temperature ceramic sintering, ACS Appl. Mater. Inter. 8 (2016) 20909–20915.
[24] J. Ma, H. Li, H. Wang, C. Lin, X. Wu, T. Lin, X. Zheng, X. Yu, Composition, microstructure and electrical properties of $K_{0.5}Na_{0.5}NbO_3$ ceramics fabricated by cold sintering assisted sintering, J. Eur. Ceram. Soc. 39 (2019) 986–993.
[25] E. Zhao, J. Hao, X. Xue, M. Si, J. Guo, H. Wang, Rutile TiO_2 microwave dielectric ceramics prepared via cold sintering assisted two step sintering, J. Eur. Ceram. Soc. 41 (2021) 3459–3465.
[26] W.M. Haynes, CRC Handbook of Chemistry and Physics, CRC Press, FL, 2017.
[27] S.J. Penn, N.M. Alford, A. Templeton, X.R. Wang, M.S. Xu, M. Reece, K. Schrapel, Effects of porosity and grain size on the microwave dielectric properties of sintered alumina, J. Am. Ceram. Soc. 80 (1997) 1885–1888.
[28] X.Q. Song, W. Lei, Y.Y. Zhou, T. Chen, S.W. Ta, Z.X. Fu, W.Z. Lu, Ultra-low fired fluoride composite microwave dielectric ceramics and their application for $BaCuSi_2O_6$-based LTCC, J. Am. Ceram. Soc. 103 (2020) 1140–1148.
[29] B. Liu, L. Li, K.X. Song, M.M. Mao, Z. Lu, G. Wang, L. Li, D. Wang, D. Zhou, A. Feteira, I.M. Reaney, Enhancement of densification and microwave dielectric properties in LiF ceramics via a cold sintering and post-annealing process, J. Eur. Ceram. Soc. 41 (2021) 1726–1729.
[30] B. Liu, K. Sha, Y.Q. Jia, Y.H. Huang, C.C. Hu, L. Li, D. Zhou, K.X. Song, High quality factor cold sintered LiF ceramics for microstrip patch antenna applications, J. Eur. Ceram. Soc. 41 (2021) 4835–4840.
[31] B. Liu, K. Sha, M.F. Zhou, K.X. Song, Y.H. Huang, C.C. Hu, Novel low-εr MGa_2O_4 (M= Ca, Sr) microwave dielectric ceramics for 5G antenna applications at the Sub-6 GHz band, J. Eur. Ceram. Soc. 41 (2021) 5170–5175.
[32] W.C. Chew, J.A. Kong, Effects of fringing fields on the capacitance of circular microstrip disk, IEEE T. Microw. Theory 28 (1980) 98–104.